

Broadband Spectral Analysis of Aql X-1

Harsha Raichur^{*}, Ranjeev Misra and Gulab Dewangan

Inter-University Centre for Astronomy and Astrophysics, Post Bag 4, Ganeshkhind, Pune-411007, India

Accepted.....; Received

ABSTRACT

We present the results of a broadband spectral study of the transient Low Mass X-ray Binary Aql X-1 observed by *Suzaku* and *Rossi X-ray Timing Explorer* satellites. The source was observed during its 2007 outburst in the High/Soft (Banana) state and in the Low/Hard (Extreme Island) state. Both the Banana state and the Extreme Island state spectra are best described by a two component model consisting of a soft multi-colour blackbody emission likely originating from the accretion disk and a harder Comptonized emission from the boundary layer. Evidence for a hard tail (extending to ~ 50 keV) is found during the Banana state; this further (transient) component, accounting for atleast $\sim 1.5\%$ of the source luminosity, is modeled by a power-law. Aql X-1 is the second Atoll source after GX 13+1 to show a high energy tail. The presence of a weak but broad Fe line provides further support for a standard accretion disk extending nearly to the neutron star surface. The input photons for the Comptonizing boundary layer could either be the disk photons or the hidden surface of the star or both. The luminosity of the boundary layer is similar to the disk luminosity in the banana state and is about six times larger in the extreme island state. The temperature of the Comptonizing boundary layer changes from ~ 2 keV in the banana state to ~ 20 keV in the extreme island state.

Key words: X-rays: binaries, Aql X-1; Star: Neutron star; accretion, accretion disks

1 INTRODUCTION

Low mass X-ray binaries (LMXB) containing weakly magnetised neutron stars (NS) are classified into Z and Atoll sources (Hasinger & van der Klis 1989; van der Klis 2006). The classification is based upon the different tracks these two types of sources trace in the colour-colour diagrams (CD) and their associated timing properties in the different spectral states. Even though detailed timing and spectral differences between the two class of sources are not completely explained, higher accretion rate is generally believed to characterise the Z as compared to the Atoll sources. Atoll sources have lower luminosities (0.001 - $0.5 L_{Edd}$) than Z sources and they have fragmented CD consisting of banana state (BS) and Extreme island state (EIS). There is also a transitional state between these two states referred to as Island state. In the BS the source luminosity is high and the observed energy spectrum is soft (high/soft state). On the other hand in the EIS the source luminosity is low and the observed energy spectrum is hard (low/hard state).

Irrespective of the type of source, there are two different approaches to model their energy spectra, both consisting of a soft/thermal and a hard/Comptonized compo-

nent (see Barret 2001, for a review). In one approach the accretion disk is considered to be emitting the soft thermal component while the boundary layer emits the hard Comptonised component (“Eastern Model” Mitsuda et al. 1989). In the other approach, the boundary layer emits the soft thermal component and the inner hot accretion disk emits the hard Comptonised component of the spectrum (“Western Model” White, Stella, & Parmar 1988). To distinguish between these two approaches good quality broadband spectral data is required. Beppo-SAX broadband (0.1-200 keV) observations show that Eastern-like models are preferred for several NS-LMXB (e.g. Guainazzi et al. 1998; Lavagetto et al. 2004; Tarana, Bazzano & Ubertini 2008).

Suzaku observations cover a broad energy range of 0.7-70 keV with good spectral resolution. This capability of *Suzaku* allows to distinguish between several modelling approaches for NS-LMXBs: Eastern-like, as in the case of the Z-source LMC X-2 (Agrawal & Misra 2009); Western-like, as in the case of the periodic burster XB1323-619 (Bałucińska-Church et al. 2009); scattered-in dust emission plus direct NS and/or disk blackbody emission, as for the eclipsing LMXB SAX J1745.6-2901 (Hyodo et al. 2009).

Aql X-1 is a recurrent soft transient LMXB with an optical companion star of $V = 21.6$ K7V spectral type (Chevalier et al. 1999) and orbital period 18.9 hours

^{*} E-mail: harsha@iucaa.ernet.in

Table 1. Suzaku observation details

Suzaku Obs Id	Suzaku Obs Start time (MJD)	Suzaku Obs Exposure (s)	Source count rate from Suzaku obs(cnt/s) [†]		Corresponding RXTE Obs Id	RXTE Obs Start time (MJD)
			XIS	PIN		
402053010 (BS)	54371.64	13825	139.90 ± 0.18	1.13 ± 0.01	None	-
402053020 (EI1)	54376.99	15132	13.27 ± 0.02	0.79 ± 0.01	93405-01-04-01	54376.98
402053030 (EI2)	54382.21	19711	15.77 ± 0.02	0.96 ± 0.01	93405-01-05-01	54382.34
402053040 (EI3)	54388.33	17915	12.10 ± 0.02	0.79 ± 0.01	93405-01-06-00	54388.36

[†] Errors quoted on count rates are 1 sigma errors

(Welsh, Robinson, & Young 2000). The distance to the source is estimated to be anywhere between 4 kpc to 6.5 kpc (Rutledge et al. 2001). The recurrent transient X-ray outbursts observed are thought to occur due to thermal instabilities in the accretion disk (van Paradijs 1996). In Aql X-1 the typical outburst recurrence time is 200 days, with average durations of 40-60 days (Šimon 2002). The source also shows Type-I X-ray bursts which are believed to be run away thermonuclear burning of the matter accreted onto the surface of the NS (Lewin, van Paradijs & Taam 1995; Bildsten 1998). High frequency quasi periodic oscillations (QPOs) between 750-830 Hz and burst oscillations have also been discovered in this source (Zhang et al. 1998). Recently an episode of coherent pulsations at 550.27 Hz lasting for 150s was discovered during the peak of the 1998 outburst (Casella et al. 2008). The occurrence of Type-I bursts, burst oscillations and the coherent pulsations in Aql X-1 confirm that the compact object is a rapidly spinning neutron star. Reig, van Straaten, & van der Klis (2004) analysed five X-ray outbursts of Aql X-1 observed using RXTE-PCA between 1997 February to 2002 May. They conclude from their timing and spectral studies that this is an Atoll source.

Here we study the broad band spectrum of Aql X-1 using the pointed *Suzaku* and *Rossi X-ray Timing Explorer* (RXTE) observations.

2 OBSERVATION AND ANALYSIS

Aql X-1 went into outburst during August 2007 and was observed using *Suzaku* (Mitsuda et al. 2007) and RXTE (Jahoda et al. 1996). The source flux increased from ~ 10 mCrab to ~ 0.2 Crab during the outburst before it finally decays to a flux of ~ 5 mCrab. Figure 1 shows the one day averaged RXTE All Sky Monitor (ASM; Levine et al. 1996) light curve of this outburst. Seven pointed observations are made using *Suzaku*. The X-ray Imaging Spectrometer (XIS; Koyama et al. 2007) was operated in the 1/4 window mode during all observations. An additional 0.5s burst option was used during the first observation (Obs Id 402053010). Since all these observations were done after November 9, 2006 no XIS2 data are available. Hard X-ray Detector (HXD; Takahashi et al. 2007) observations were done with XIS nominal pointing. For the last two *Suzaku* observations the count rates are low and the spectra obtained from XIS and HXD have poor statistics. The fifth *Suzaku* observation data could not be analysed since the attitude file provided by the HEASARC site is corrupted.

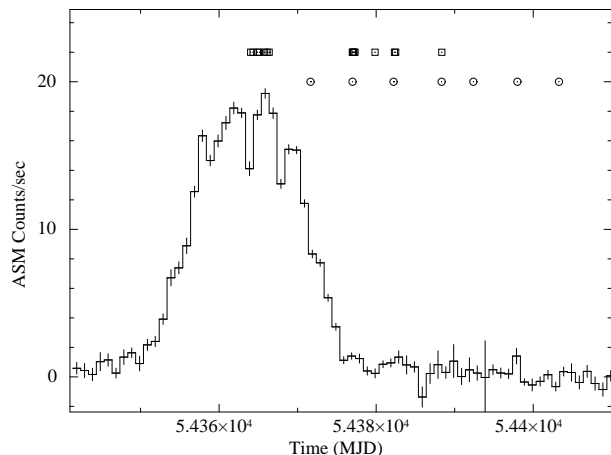


Figure 1. Figure shows the outburst light curve of Aql X-1 as observed using the RXTE-ASM (1.5-12 keV). The square points marked at the top of the figure show the times of RXTE-PCA observations and the circled points below the squares show the times of *Suzaku* observations. We note here that a flux of 1 Crab corresponds to ~ 75 ASM counts/s (Levine et al. 1996).

Hence these three observations are not used for the work presented here. For more details see Table 1.

There are 16 pointed RXTE Proportional Counter Array (PCA) observations between 54360 MJD and 54400 MJD, seven during the peak of the outburst and nine after the decay of the outburst (Figure 1). Three of the PCA observations are simultaneous to the second, third and fourth *Suzaku* observations (Table 1). In the following subsections we give the analysis details of data reduction for RXTE PCA and *Suzaku* respectively.

2.1 RXTE-PCA

PCA data are used to create the CD of Aql X-1 for the 2007 outburst. To normalise the Aql X-1 colours by Crab colours we used the three PCA Crab observations between 54360 MJD and 54400 MJD. Background subtracted lightcurves of Aql X-1 and Crab were extracted using Std2 mode data in energy bands 3.0-4.5 keV, 4.5-6.0 keV, 6.0-9.7 keV, 9.7-16.0 keV with 16s time resolution. To eliminate artifacts that may arise due to different gain corrections for the different PCUs only photons collected in the third PCU were used since this PCU was on during all the observations. The Soft colour (SC) is defined as the ratio of count rates in en-

ergy bands 4.5-6.0 keV and 3.0-4.5 keV and the Hard colour (HC) as the ratio of count rates in energy bands 9.7-16.0 keV and 6.0-9.7 keV. Average Crab colours obtained are $SC = 1.986 \pm 0.002$ and $HC = 0.5992 \pm 0.0007$. Figure 2 is the CD obtained by plotting normalised Aql X-1 HC versus SC. All normalised Aql X-1 colours having error greater than 5% of the observed colour were ignored. This amounted in rejecting 14 out of 307 points of the CD. From Figure 2 we conclude that during the second, third and fourth *Suzaku* observations, Aql X-1 was in the EIS (compare Figure 2 of this paper with Figure 2 of Reig, van Straaten, & van der Klis 2004) We will refer to these three *Suzaku* observations as EI1, EI2, EI3 respectively. It is noted that EI2 observation has the best statistics in the EIS and also EI2 is brighter than EI1 indicating irregular decline in the lightcurve (Table 1).

There are no simultaneous PCA observations during the first *Suzaku* observation to ascertain the spectral state of the source. Hence we use a different method to find the normalised Aql X-1 SC and HC during this observation. The best fit spectral model that can reproduce the observed *Suzaku* spectrum is used to simulate a PCA spectrum. The `fakeit` command of XSPEC package is used for this simulation. Average count rates in the four energy bands required to calculate the SC and HC are obtained by this simulated PCA spectrum. Aql X-1 SC and HC thus obtained are normalised by the average Crab SC and HC respectively. In figure 2 the point marked by an open plus sign with error bars represents this normalised Aql X-1 SC and HC. Thus we conclude that during the first *Suzaku* observation, Aql X-1 was in the BS. Henceforth this observation will be referred to as the BS observation.

The PCA spectra from simultaneous observations (Table 1) are used for comparison with the *Suzaku* spectra. We have used the Std2 spectra and response files provided in the standard products. Energy channels were appropriately regrouped before the final spectral fitting.

2.2 *Suzaku*

For each front-illuminated XIS detector (XIS0 and XIS3) we extracted the source spectra using a 260 arc-sec circular extraction region centered on the source. The energy scale is reprocessed using the `xispi` task. Background spectra are extracted using appropriate circular regions outside the source region. Corresponding response files are generated using the `xismfgen` and `xissimarfgen` tools. The spectra from respective XIS0 and XIS3 detectors are then added together using the `addascaspec` tool.

During high count rates, as is the case for the BS observation, there is a possibility of pile-up in the XIS detectors. To check for pile-up we extracted the source spectrum from an annular region with inner radius of 40 arc-sec and an outer radius of 260 arc-sec. Corresponding response files were also generated. Figure 3 shows the ratio of XIS0 background subtracted spectrum extracted from the full circular region and from the annular region. The constant ratio indicates that both these spectra are similar and differ only in the observed count rates. Similar result is seen for XIS3 detector also. This confirms that the BS observation is not affected by pile-up.

The data processing version used for the HXD cleaned

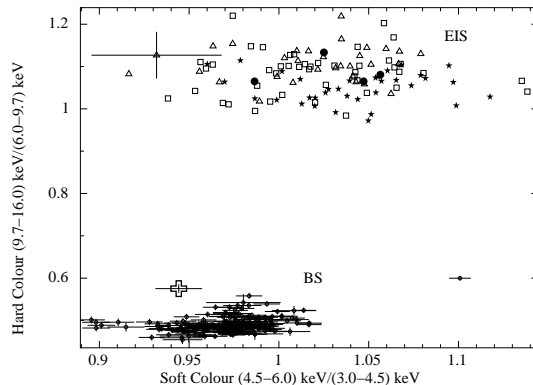


Figure 2. Figure shows Colour-Colour diagram of Aql X-1 for the 2007 outburst. The open circles with error bars are points during the peak of the outburst where no *Suzaku* observations are available. Points marked with filled circles, filled stars and triangles are from RXTE observations simultaneous to the second, third and fourth *Suzaku* observations respectively. Note that there are no RXTE observations close to the first *Suzaku* observation. Points marked with rectangles are remaining RXTE observations after the decay of the outburst where no simultaneous *Suzaku* observations are available. The point marked with an open plus sign and error bars is obtained from the PCA spectra simulated using the best fit model for the first *Suzaku* observation. Error bars on points representing the EIS of Aql X-1 are suppressed for clarity except one point in the upper left hand corner.

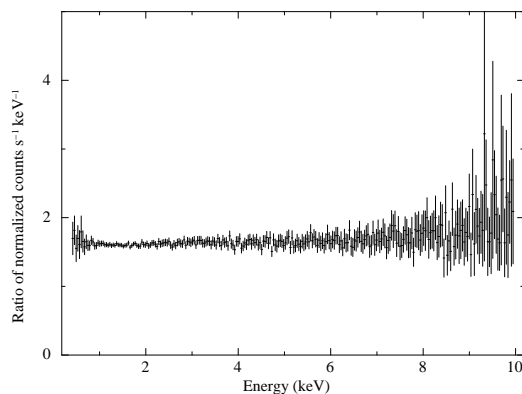


Figure 3. Figure shows a plot of the ratio of XIS0 spectrum for BS observation, obtained using a full circular source region of radius 260 arc-seconds to the spectrum obtained from an annular region of inner radius 40 arc-seconds and outer radius of 260 arc-seconds at different energies. The constant ratio implies that both these spectra differ only in the observed count rates and there is no pile-up at the centre of the CCD during the BS observation.

products is 2.1.6.15. Hence the PIN spectra are extracted using the cleaned event files following the standard analysis threads on the *Suzaku* website.¹ The PIN non-X-ray background is extracted from the observation specific model provided by the instrument team. It is combined with the standard model for cosmic X-ray background. Appropriate response files for XIS nominal pointing available from the

¹ <http://heasarc.nasa.gov/docs/suzaku/analysis/abc/>

Table 2. XSPEC Model Components used

Model	XSPEC Components
M1 (a/b)	$C^\dagger \times \text{wabs} (\text{diskbb} + \text{diskline} + \text{nthcomp})^{a,b}$
M2	$C^\dagger \times \text{wabs} (\text{BBody}/\text{BBodyrad} + \text{nthcomp})$

†: Constant used to get relative normalisation between XIS and HXD spectra

a: The input photons to nthcomp are from accretion disk

b: The input photons to nthcomp are from an hidden blackbody emitting NS surface

calibration database CALDB (version XIS-20101108, HXD-20101202) are used.²

The XIS spectra are grouped such that the final spectra have ~ 250 energy channels so that there are about three channels per energy resolution of $\sim 150\text{eV}$. Energy channels corresponding to the energy range of 1.75-1.95 keV are ignored since the response files do not adequately remove the absorption edge present in this energy range. Ten consecutive energy channels are grouped into one energy channel of the final grouped PIN spectrum. The net count rates for the XIS and PIN spectra are given in Table 1. We use XSPEC V12.5.1n to fit the spectral models to the observed X-ray spectrum.

3 RESULTS

We have used two different phenomenological models to describe the observed spectra of the source in both the EIS and BS. In the first model (henceforth referred to as M1) we model the soft component using multi-temperature disk blackbody (DBB) and the hard component as Comptonised emission from the boundary layer. The hot boundary layer is assumed to completely cover the neutron star surface. This Eastern-like model has two variants. One, where the input photons to the boundary layer are from the accretion disk (M1a) and second where the input photons are from the underlying blackbody emission of the neutron star surface (M1b). The presence of a standard accretion disk allows for the possibility of a broad Iron line emission in this model which we include using the XSPEC model “diskline”. In the second Western-like model (M2) we model the soft component using a single-temperature blackbody (BB) emitted from the boundary layer. The hard component is modelled as Comptonised emission from an inner hot disk where the input photons are from the boundary layer.

The Comptonised spectra for both the models is represented by the XSPEC function “nthcomp” (Zdziarski, Johnson & Magdziarz 1996; Życki, Done & Smith 1999). We apply this Comptonization model mainly because it can have input seed photon populations of different nature and distribution (pure blackbody, multicolour disk) thus allowing to test different emission geometries. In the M1a model the input photon distribution is due to disk blackbody and hence the input temperature is set equal to the maximum temperature

of the disk blackbody emission. In the M2b model, input photon distribution is due to the blackbody emission from the NS surface and hence the input temperature is a free parameter. On the other hand in the M2 model, the photon distribution is due to neutron star boundary layer and hence of a blackbody shape and the input temperature is set equal to the temperature of this neutron star boundary layer.

A multiplicative component (“wabs”) is introduced in all spectral fitting to model the absorption of the source spectrum by intervening material along the line sight. We note here that the average Dickey & Lockman nH value in the direction of Aql X-1 is $0.33 \times 10^{22} \text{ cm}^{-2}$. The nH values obtained in our fits agree with this average value. Another constant multiplicative term is used in both the models for the relative normalisation of the XIS and corresponding HXD spectra. The cross-calibration constant for XIS nominal pointing as suggested by the Suzaku team is 1.16 ± 0.014 ^{3,4}. The value for the constant that we get from our fits agree with those suggested by the Suzaku team within errors. The XSPEC model components used for M2 and M1 are tabulated in Table 2. While fitting the near simultaneous *RXTE* spectra, we fix the absorbing column density, nH to the corresponding nH value derived from the *Suzaku* spectral fit since *RXTE* data alone cannot constrain the nH value.

The normalisation parameter of the XSPEC BBody component gives the blackbody luminosity L_{BB} and the normalisation parameter of the XSPEC BBodyrad component gives the blackbody radius R_{BB} . Similarly from the parameter values of the XSPEC nthcomp component we can estimate the total Compton luminosity L_{comp} , the required luminosity of the input photons L_{inp} , the amplification factor (A) and when kT_{bb} is a free parameter the radius of the blackbody R_{BB} . From the XSPEC diskbb model we calculate the inner accretion disk radius (R_{in}) and the disk luminosity L_{DBB} . The calculated values of these parameters allow us to constrain the two models considered here. Note that throughout this paper for calculating luminosities we use distance to the source as $D = 5.25 \pm 1.25 \text{ Kpc}$ (Rutledge et al. 2001) and the error quoted for luminosities take into account this uncertainty in the distance.

The results from the observations EI1, EI2 and EI3 when the source was in the EIS will be presented together in the next sub-section and that of the BS in the subsequent one.

3.1 Spectral analysis of Aql X-1 during the Extreme Island State

We start with analysing the *Suzaku* spectra using Model M1a. If the Iron line emission is omitted the best fit χ^2/ν obtained are 284.50/241, 295.74/237 and 305.31/241 for observations EI1, EI2 and EI3 respectively. Adding a Gaussian line at 6.4 keV improves the fit considerably. The width of the Gaussian turns out to be $> 0.5 \text{ keV}$, indicating the line is broad. Hence, we adopt the more physical “diskline” model

² http://heasarc.gsfc.nasa.gov/docs/heasarc/caldb/suzaku/docs/suzaku_caldbhistory.html

³ <http://www.astro.isas.jaxa.jp/suzaku/doc/suzakumemo/suzakumemo-2007-11.pdf>

⁴ <http://www.astro.isas.jaxa.jp/suzaku/doc/suzakumemo/suzakumemo-2008-06.pdf>

Table 3. Parameter values with respective 1σ errors for model M1a during the EIS

M1a Parameter	EI1		EI2		EI3	
	402053020	93405-01-04-01	402053030	93405-01-05-01	402053040	93405-01-06-00
$nH(10^{22})\text{cm}^{-2}$	0.311 ± 0.008	0.311(frozen)	0.287 ± 0.007	0.287(frozen)	0.445 ± 0.009	0.445(frozen)
$T_{in}(\text{keV})$	0.85 ± 0.02	0.85 ± 0.11	0.82 ± 0.02	0.97 ± 0.09	0.82 ± 0.02	0.79 ± 0.05
$L_{DBB}(10^{35}\text{erg/s})$	5.1 ± 2.4	5.0 ± 2.5	4.7 ± 2.2	6.9 ± 3.2	5.2 ± 2.5	6.9 ± 3.3
$R_{in}^{\dagger}(\text{km})$	6.6 ± 0.2	6.8 ± 1.1	6.7 ± 0.2	5.9 ± 0.9	7.1 ± 0.2	9.0 ± 1.1
γ	1.71 ± 0.04	1.85 ± 0.05	1.78 ± 0.03	1.73 ± 0.04	1.71 ± 0.05	1.74 ± 0.04
$kT_e(\text{keV})$	20.0(frozen)	20.0(frozen)	20.0(frozen)	20.0(frozen)	$13.6^{+4.9}_{-2.3}$	$9.7^{+2.9}_{-1.7}$
$L_{comp}(10^{35}\text{erg/s})$	25.5 ± 12.1	25.4 ± 12.1	29.4 ± 14.0	30.6 ± 14.5	21.8 ± 10.4	19.8 ± 9.4
$L_{inp}(10^{35}\text{erg/s})$	4.6 ± 2.2	6.1 ± 2.9	6.1 ± 2.9	6.1 ± 2.9	4.3 ± 2.0	4.6 ± 2.2
A	5.54	4.16	4.82	5.01	5.07	4.30
C^{\ddagger}	1.05 ± 0.06	-	1.11 ± 0.05	-	1.10 ± 0.07	-
χ^2/ν	266.70/240	30.48/28	260.93/236	37.03/28	287.22/240	24.23/23

\dagger Propagating distance errors in calculating error on R_{in} would increase the errors to ~ 5 km for all observations.

\ddagger C is the cross-calibration constant between the XIS and HXD spectra.

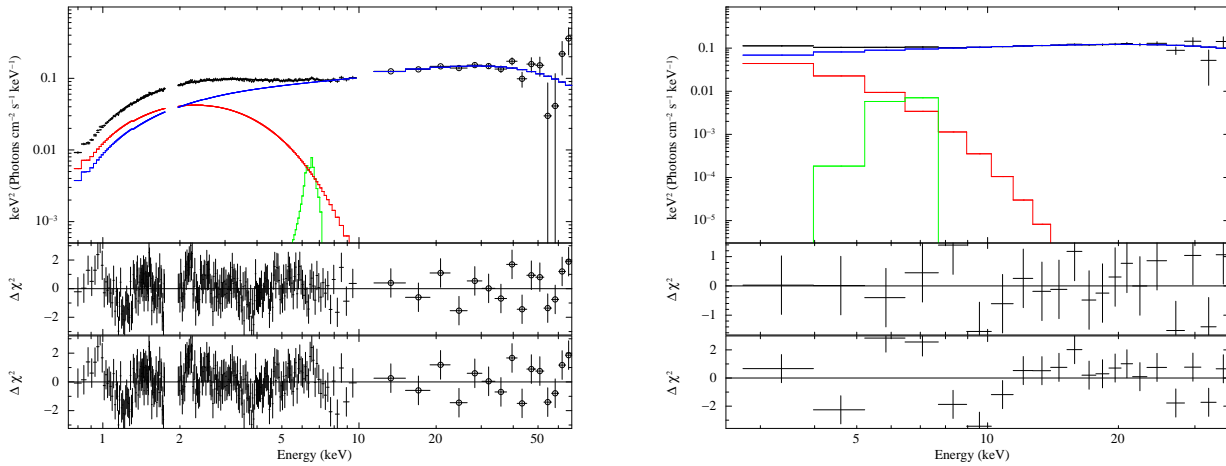


Figure 4. The left hand panel shows the *Suzaku* and the right hand panel shows the corresponding RXTE-PCA unfolded spectrum for the EI3 observation. Observed data points are marked in black. In the left panel points below 10 keV are from the XIS detector and the points marked with a circle are from the HXD detector. Red line shows the contribution from the disk blackbody component, the Blue line shows the contribution of the Comptonised component and the green line shows the contribution from the Fe line. The bottom panels show the residues as a function of energy with (middle panel) and without (bottom panel) the Fe line.

to represent the Iron line. However, the data is not good enough to constrain all the parameters of the model and hence we fix some of them (emissivity index $\beta = -2.0$, inclination angle $i = 45^\circ$, inner radius $R_{in} = 10\text{GM}/c^2$ and outer radius $R_{out} = 1000\text{GM}/c^2$). Thus only the normalisation of the line is a fitted parameter. The same model is applied to near simultaneous *RXTE* observations. Removing the Iron line component for the *RXTE* spectra, gives best fit χ^2/ν values of 38.39/29, 70.08/29, 64.21/24 for Obs. Id. 93405-01-04-01/05-01/06-00 respectively, which are significantly higher than χ^2 obtained with the line feature. Thus, the Iron line feature is detected both in the *Suzaku* as well as in the *RXTE* spectra.

The electron temperature of the Comptonizing boundary layer component, kT_{in} is unconstrained for observations EI1 and EI2 for both *Suzaku* and *RXTE* data with a lower limit of above 15keV. Hence we fix $kT_{in} = 20$ keV for these observations. The spectral parameters and the best fit χ^2/ν obtained for the *Suzaku* and *RXTE* spectra are given in Table 3. Figure 4 shows the $E^2F(E)$ spectrum for *Suzaku* ob-

servation EI3 and corresponding RXTE spectrum along with the M1a model components. Note that the best fit spectral parameters are consistent within errors for the *Suzaku* and *RXTE* observations for all three sets. This similarity and consistency between the two different instruments, shows that the spectral extraction and response generation is robust and correct.

The inner radius of the accretion disk turns out to be ~ 7 km which is rather small since it needs to be larger than the radius of the neutron star $R_s \sim 10$ km. However, this may be due to the uncertainty in the distance to the source. Assuming that the distance is 6.5 instead of 5.25 kpc used here would lead to physically acceptable inner radii of > 10 km. Moreover, the colour factor assumed here is $f = 1.7$ and a slightly higher value could also correct this discrepancy. Note that the luminosity of the disk is of the same order as the input luminosity into the Comptonizing medium. This is an important consistency check since the model assumes that input photons arise from the accretion disk.

Next we consider the possibility that the input photons

to the Comptonizing medium arise from a blackbody emission of the underlying neutron star surface (Model M1b). Thus in this model temperature of the blackbody emission, kT_{bb} is an extra free parameter. The best fit χ^2/ν values are 268.35/239, 266.18/235 and 260.83/239 for EI1, EI2 and EI3 observations respectively. The *RXTE* spectral fits are also consistent with the *Suzaku* fits, although the extra freedom of kT_{bb} does not allow the spectral parameters to be well constrained. But it is noted that for EI1 and EI2, the values of kT_{bb} and T_{in} coincide within errors whereas for EI3 $kT_{bb} < T_{in}$ which is not compatible with the geometry of this model. The calculated inner disk radii values for this model turn out to be larger at ~ 9 km. However, the radius of the blackbody assumed to be from the neutron star surface, turns out to be rather small (~ 5 km) for the first two observations, namely EI1 and EI2. Again, physical consistency may be obtained by using a larger distance to the source and/or including a colour factor in the blackbody radius calculation. Also for the EI3 observation, the obtained radius of the blackbody is $R_{BB} = 18 \pm 5$ km which is greater than the calculated inner disk radius $R_{in} = 7.5 \pm 0.3$ km. Therefore, perhaps the more physical picture for EIS is that the input photons for Comptonization are mainly contributed by the accretion disk making M1a model more feasible than the M1b model in this case.

We consider next the alternate geometry where the Comptonised component arises from an inner hot disk and the boundary layer produces a blackbody emission (Model M2). When this model is used to fit the three EIS spectra the best fit χ^2/ν for observations EI1, EI2 and EI3 are 300.87/241, 306.83/237 and 267.50/241 respectively. In this model the input photon temperature for Comptonization component kT_{bb} is kept equal to the corresponding blackbody temperature kT . The calculated blackbody radius R_{BB} for the three observations are 3.6 ± 0.9 , 3.5 ± 0.8 and 4.1 ± 1.0 km respectively. These values are significantly smaller than the neutron star radius of ~ 10 km. The values can be made consistent only by assuming a large distance to the source of > 11 kpc or by assuming an unphysical large colour factor of ~ 3 . Note that for a radius of 3 km the emitting region is only one-tenth the neutron star surface. This makes the geometry unfavourable as compared to the M1 model.

Moreover, the χ^2 values obtained are significantly larger than the ones obtained for M1 models. Even if we include a broad Iron line (which in the absence of a cold disk may not be physical) the χ^2/ν values are 293.99/239, 285.49/235 and 260.46/239 which are higher than the ones obtained for the M1 model. Consistent results are obtained from the *RXTE* data which provide χ^2/ν of 34.40/28, 87.43/29 and 24.33/23 respectively, again significantly higher than what was obtained earlier.

3.2 Spectral analysis of Aql X-1 during the Banana State

We now come to the spectral analysis of the first *Suzaku* observation taken during the decline of the 2007 Aql X-1 outburst. During this observation the overall X-ray source flux is higher than that during the next three observations when the source is in the EIS. It was seen that for this BS *Suzaku* spectrum there is an excess of count rate at the high

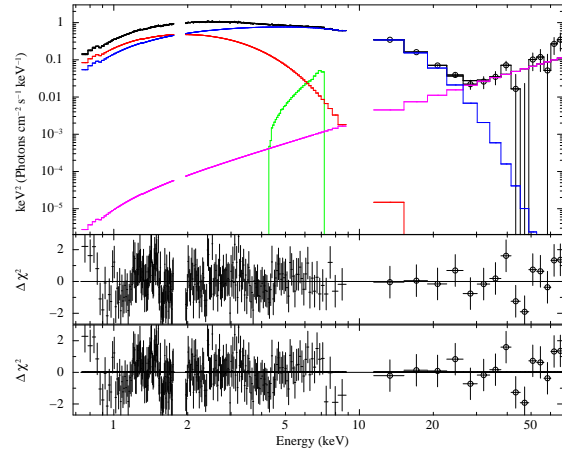


Figure 5. The M1a model spectral components (listed in Table 4 along with the unfolded spectrum for the BS *Suzaku* observation. Black points below 10 keV show the XIS spectrum and black points marked with circles show the HXD spectrum. The multicoloured disk blackbody component is shown in red, the Comptonised component is shown in blue, the power-law component in magenta and the Fe line component in green. The bottom panels show residues as a function of energy with (middle panel) and without (bottom panel) Fe line.

energy end of the spectrum which could not be modelled by thermal Comptonization. We have added a hard power-law component (with photon index $\Gamma = 0$) to all spectral fitting to account for the high energy excess. We note here that energy contribution of this component diverges with energy and hence there should be a cutoff at both the high and low energy end. But for the given data neither the photon index nor the cutoffs at low and high energies could be constrained. Therefore luminosity contributed by this component has been calculated only in the energy range of 0.7–70.0 keV in which the spectral fitting has been performed.

Table 4 lists the best fit parameters for the variations of the cold accretion disk model (M1a/b) while Figure 5 shows the unfolded spectrum with the different components for the M1a model. The electron temperature of the Comptonizing region is smaller ($kT_e \sim 2.3$ keV) as expected and the inner radius of the accretion disk is significantly larger at ~ 40 km. As in the EIS fitting, the disk luminosity is nearly equal to the input luminosity (as expected in this geometry), although the luminosities have increased by nearly an order of magnitude. Here, in M1b model, the radius of the underlying neutron star, $R_{BB} \sim 10$ km, which is larger (and hence more physical) than that obtained for the EIS state. Note that the high energy power-law component contributes around 1.5% of the total luminosity. Without this component the χ^2/ν is 282.81/234 for M1a model and 279.90/233 for M2b model. For both M1a and M1b model, the emissivity index of the “diskline” model can be constrained to $q \sim -3$.

The alternate geometry of an hot inner disk (M2) provides an unacceptably larger χ^2/ν of 359.99/235. The inclusion of a broad Gaussian for the Iron line (which may not be physical given the absence of a cold disk) reduces it to 338.43/233, which is still significantly higher than what is obtained for the M1 models. However, in this case the radius of the blackbody emitting boundary layer turns out to be ~ 18 km and hence is physically possible.

Table 4. Parameter values of model M1(a/b) for Obs Id 402053010

M1 Parameter	M1a Values	M1b Values
$nH(10^{22}) \text{ cm}^{-2}$	0.370 ± 0.009	0.366 ± 0.008
$T_{in}(\text{keV})$	0.66 ± 0.02	0.71 ± 0.02
$L_{DBB} \text{ (erg/s)}$	$(5.8 \pm 2.8) \times 10^{36}$	$(10.3 \pm 4.9) \times 10^{36}$
$R_{in} \text{ (Km)}^a$	37.1 ± 1.3	43.1 ± 1.7
Γ^b	0.0(frozen)	0.0(frozen)
$L_{PL}^c \text{ (erg/s)}$	$(2.6 \pm 1.2) \times 10^{35}$	$(2.7 \pm 1.3) \times 10^{35}$
γ	1.94 ± 0.09	$2.1^{+0.6}_{-0.3}$
$kT_e \text{ (keV)}$	2.3 ± 0.1	$2.4^{+0.2}_{-0.1}$
$kT_{bb} \text{ (keV)}$	$= T_{in}$	$1.1^{+0.3}_{-0.4}$
$L_{comp} \text{ (erg/s)}$	$(10.6 \pm 5.0) \times 10^{36}$	$(6.1 \pm 2.9) \times 10^{36}$
$L_{inp} \text{ (erg/s)}$	$(4.6 \pm 2.2) \times 10^{36}$	$(4.3 \pm 2.1) \times 10^{36}$
A	2.30	1.41
$R_{BB} \text{ (Km)}^d$	-	9.5 ± 6.9
q	$-3.1^{+0.6}_{-1.7}$	$-3.1^{+0.7}_{-4.7}$
C	1.19 ± 0.09	1.16 ± 0.08
χ^2/ν	246.78/233	246.10/232

a: Propagating error on distance increases error in R_{in} to 25 km for M1a and to 29 km for M1b.

b: The power law should have both a low and high energy cut-off which cannot be constrained by the present data.

c: Luminosity due to the powerlaw tail is calculated in the energy range 0.7-70.0 keV. See results section for more details.

d: Propagating error on distance increases error in R_{BB} to 7.2 km.

4 SUMMARY AND DISCUSSION

In this work, we analyse *Suzaku* and *RXTE* observations of Aql X-1, to constrain the geometry of the source in both the low flux EIS and high flux BS, and to report the discovery of a hard X-ray tail in the BS. In particular, a standard accretion disk with a hot Comptonizing boundary layer whose input photons are from the disk is the preferred geometry for both states. The alternate model of a hot Comptonizing inner disk and a blackbody emitting boundary layer gives significantly larger χ^2 for all four *Suzaku* observations including three nearly simultaneous *RXTE* observations. Moreover, for the EIS observations, the radius of the blackbody emitting boundary layer turns out to be unphysically small, ~ 3 km. The presence of a broad Iron line feature provides further support for the existence of a cold accretion disk in the source. The preferred geometry is the same as inferred from broad band study of many other NS-LMXBs (Barret 2001) and hence seems to be general.

For all observations, the luminosity of the input photons to the Comptonizing hot boundary layer is similar to that of the disk and hence it is possible that the main source of input photons is the disk itself. While it may also be possible that the source of soft photons could be the underlying blackbody emitting neutron star, statistically the data cannot differentiate between these scenarios.

Our results confirm that the electron temperature of the Comptonizing boundary layer in EIS is higher as compared to same in the BS. Also the inner radius of the accretion disk is higher during the BS observation. The spectral slope $\gamma \sim 1.8$ remains nearly constant, implying that the optical depth has increased in the high flux state. In the “nthcomp” model,

the optical depth of the medium, for a spherical geometry can be estimated by (Sunyaev & Titarchuk 1980)

$$\Gamma_{thcomp} = \left[\frac{9}{4} + \frac{1}{(kT_e/m_e c^2)\tau(1 + \tau/3)} \right]^{1/2} - \frac{1}{2} \quad (1)$$

The optical depth $\tau \sim 2$ for the observations EI1 and EI2 and ~ 5 for the EI3 observation. In the BS $\tau \sim 13$. The difference in the electron temperature is the primary cause for the two states to have different locations in the colour-colour diagrams. A larger number of observations, sampling the source at different times of the outburst will provide more information regarding the complete temporal evolution of the source.

For the EISs, when the input photons are assumed to be from the disk (Table 3), the luminosity of the disk is $\sim 5 \times 10^{35} \text{ ergs s}^{-1}$. The luminosity of the boundary layer, which is the luminosity in the Comptonised component minus the input luminosity $L_{comp} - L_{inp}$, is $\sim 2.5 \times 10^{36} \text{ ergs s}^{-1}$. Thus energy released in the boundary layer is about 5 times larger than that of the disk. When the input photons are taken to be the underlying neutron star surface, boundary layer luminosity, $L_{comp} \sim 2.8 \times 10^{36} \text{ ergs s}^{-1}$ is about a factor of four more than the disk luminosity $\sim 7 \times 10^{35} \text{ ergs s}^{-1}$. For the BS this ratio is ~ 1 when the input photons are disk photons and ~ 0.7 when they arise from the underlying star surface. Theoretically, the ratio of the energy output in the boundary layer to that of the disk can range from 1-3 depending on the spin and equation of state of the neutron star (e.g. Bhattacharyya et al. 2000). A ratio of five would imply an extremely soft equation of state. However, the simple phenomenological models used here do not warrant one to make concrete statements but one can conclude that the boundary layer is more luminous than the disk, which is consistent with the expected energy release ratio.

An interesting result is the detection of an hard X-ray power-law emission in the high flux state which is only 1.5% of the total source luminosity. Such hard tails have been detected in Z sources and only one Atoll source GX 13+1 earlier (Paizis et al. 2006). The origin of this emission is unknown and maybe due to some non-thermal emission in a jet (Migliari & Fender 2006). Indeed, a weak radio emission has been detected in the high soft state of Aql X-1 (Rupen, Mioduszewski, & Dhawan 2004), which is also observed in other atoll sources (Migliari & Fender 2006). Alternatively, the hard X-ray emission could be due to an hybrid non-thermal emission (e.g. Coppi 1999) or bulk motion Comptonization (e.g. Titarchuk, Mastichiadis & Kylafis 1997). Multiple observations of the source may reveal whether the hard X-ray tail is variable and whether it is correlated with the radio emission.

The work highlights the utility of broad band spectral analysis of LMXB. Apart from other *Suzaku* observations the upcoming Indian satellite ASTROSAT will be useful in such studies of LMXBs containing weakly magnetised neutron stars as it will provide good timing and spectral resolution.

5 ACKNOWLEDGEMENTS**REFERENCES**

- Agrawal V. K., Misra R., 2009, MNRAS, 398, 1352
- Balucińska-Church M., Dotani T., Hirotsu T., Church M. J., 2009, A&A, 500, 873
- Barret D., 2001, Advances in Space Research, 28, 307
- Bhattacharyya S., Thampan A. V., Misra R., Datta B., 2000, ApJ, 542, 473
- Bildsten L., 1998, in The Many Faces of Neutron Stars, ed. R. Buccheri, J. van Paradijs, & M. A. Alpar (Dordrecht: Kluwer), 419
- Casella P., Altamirano D., Patruno A., Wijnands R., van der Klis M., 2008, ApJ, 674, L41
- Chevalier C., Ilovaisky S. A., Leisy P., Patat F., 1999, A&A, 347, L51
- Coppi P. S., 1999, High Energy Processes in Accreting Black Holes, ASP Conference Series, Vol. 161, Pg. 375
- Guainazzi M., Parmar A. N., Segreto A., Stella L., dal Fiume D., & Oosterbroek T., 1998, A&A, 339, 802
- Hasinger, G., & van der Klis, M., 1989, A&A, 225, 79
- Hyodo Y., Ueda Y., Yuasa T., Maeda Y., Makishima K., Koyama K., 2009, PASJ, 61, 99
- Jahoda K., Swank J. H., Giles A. B., Stark M. J., Strohmayer T., Zhang W., Morgan E. H., 1996, SPIE, 2808, 59
- Koyama K., et al. 2007, PASJ, 59, 23
- Lavagetto G., Iaria R., di Salvo T., Burderi L., Robba N. R., Frontera F., Stella, L., 2004, NuPhS, 132, 616
- Levine A. M., Bradt H., Cui W., Jernigan J. G., Morgan E. H., Remillard, R., Shirey R. E., Smith D. A., 1996, ApJ, 469, 33
- Lewin W. G. H., van Paradijs J., Taam R. E., 1995, in X-ray Binaries, ed. W. H. G. Lewin, J. van Paradijs, & E. P. J. van den Heuvel (Cambridge: Cambridge Univ. Press), 175
- Migliari S., Fender R. P., 2006, MNRAS, 366, 79
- Mitsuda K., et al., 2007, PASJ, 59, 1
- Mitsuda K., Inoue H., Nakamura N., Tanaka Y., 1989, PASJ, 41, 97
- Paizis A., et al., 2006, A&A, 459, 187
- Reig P., van Straaten S., van der Klis M., 2004, ApJ, 602, 918
- Rupen M. P., Mioduszewski A. J., Dhawan V., 2004, ATel, 286, 1
- Rutledge R. E., Bildsten L., Brown E. F., Pavlov G. G., Zavlin V. E., 2001, ApJ, 559, 1054
- Šimon V., 2002, A&A, 381, 151
- Sunyaev R. A., Titarchuk L. G., 1980, A&A, 86, 121
- Takahashi T., et al., 2007, PASJ, 59, 35
- Tarana A., Bazzano A., Ubertini P., 2008, ApJ, 688, 1295
- Titarchuk L., Mastichiadis A., Kylafis N. D., 1997, ApJ, 487, 834
- van der Klis, M., 2006, in Compact Stellar X-ray Sources (eds. W. Lewin & M. van der Klis, Cambridge University Press), 39-112
- van Paradijs J., 1996, ApJ, 464, L139
- Welsh W. F., Robinson E. L., Young P., 2000, AJ, 120, 943
- White N. E., Stella L., Parmar A. N., 1988, ApJ, 324, 363
- Zdziarski A. A., Johnson W. N., Magdziarz P., 1996, MNRAS, 283, 193
- Zhang W., Jahoda K., Kelley R. L., Strohmayer T. E.,

- Swank J. H., Zhang S. N., 1998, ApJ, 495, L9
- Życki P. T., Done C., Smith D. A., 1999, MNRAS, 309, 561